Ferrocene-decorated graphene nanosheets built by edge-to-face π-π interaction for room temperature ppb-level NO sensing

Zhang, Lulu; Gao, Yixun; Feng, Yancong; Mai, Zhijian; Wang, Jianqiang; Chang, Yanwei; Wang, Fengnan; Paoprasert, Peerasak; French, Paddy J.; More Authors

DOI
10.1016/j.talanta.2024.127365

Publication date
2025

Document Version
Final published version

Published in
Talanta

Talanta 285 (2025) 127365

Contents lists available at ScienceDirect

Talanta

journal homepage: www.elsevier.com/locate/talanta

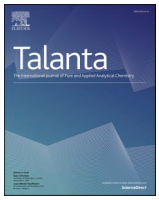

Ferrocene-decorated graphene nanosheets built by edge-to-face π-π interaction for room temperature ppb-level NO sensing

Lulu Zhang [a], Yixun Gao [a,**], Yancong Feng [a], Zhijian Mai [a], Jianqiang Wang [a], Yanwei Chang [a], Fengnan Wang [b], Hao Li [a], Peerasak Paoprasert [c], Yi-Kuen Lee [d,e], Paddy J. French [f], Ahmad M. Umar Siddiqui [g], Guofu Zhou [a], Yao Wang [a,*]

[a] National Center for International Research on Green Optoelectronics, Guangdong Provincial Key Laboratory of Optical Information Materials and Technology, Institute of Electronic Paper Displays, South China Academy of Advanced Optoelectronics, South China Normal University, Guangzhou, 510006, PR China
[b] Department of Thoracic Oncology, State Key Laboratory of Respiratory Diseases, The First Affiliated Hospital of Guangzhou Medical University, Guangzhou, 510006, PR China
[c] Department of Chemistry, Faculty of Science and Technology, Thammasat University, Pathumthani, 12121, Thailand
[d] Department of Mechanical & Aerospace Engineering, Hong Kong University of Science and Technology, Clear Water Bay, Kowloon, Hong Kong Special Administrative Region
[e] Department of Electronic & Computer Engineering, Hong Kong University of Science and Technology, Clear Water Bay, Kowloon, Hong Kong Special Administrative Region
[f] BE Laboratory, EWI, Delft University of Technology, Delft, 2628CD, the Netherlands
[g] Department of Chemistry, Faculty of Science and Arts and Promising Centre for Sensors and Electronic Devices (PCSED), Najran University, Najran, 11001, Saudi Arabia

ARTICLE INFO

Keywords:
Nitric oxide
Gas sensor
Ferrocene
Graphene
π-π interaction
Supramolecular assembly

ABSTRACT

The development of materials toward ppb-level nitric oxide (NO) sensing at room temperature remains in high demand for the monitoring of respiratory inflammatory diseases. In order to find an iron-containing molecule without steric hindrance to combine with graphene for room temperature NO gas sensing, here a supramolecular assembly of ferrocene (Fc) and reduced graphene oxide (rGO) was designed and prepared for NO sensing. The assembly of Fc/rGO was characterized using FT-IR, TEM, and XPS measurements. The Fc/rGO-based sensors exhibited superior NO sensing properties at room temperature including high response (R_a/R_g = 1.73, 1 ppm), high selectivity against other exhaled gases, reliable repeatability and stability (less than 4 % decrease after 40 days). A practical limit of detection (LOD) of 200 ppb was achieved. The theoretical simulation demonstrates that ferrocene is assembled via π-π interaction with rGO in edge-to-face configuration which provides relatively lower energy than face-to-face configuration does for the whole assembly. It was first verified that the enhanced adsorption capacity and the charge transfer between NO and Fc/rGO would result in improvement of the assembly's sensitivity toward NO after ferrocene was assembled with graphene. This work provides a fresh approach of anchoring iron on graphene for gas sensing via supramolecular methods.

1. Introduction

Nitric oxide (NO), an important signaling molecule, is widely known as playing diverse roles in regulating physiological processes [1–5]. A large amount of evidence shows that determination of fractional exhaled nitric oxide (FeNO, ppb level) is an effective non-invasive way to evaluate inflammatory respiratory diseases, which is helpful for clinical diagnosis [6,7]. However, due to the high reactivity and short half-life of NO, the exploitation of ppb-level room temperature NO gas sensors is still challenging to meet the increasing demand for clinical applications [8–10].

There are a variety of methods for detecting NO, such as chemiluminescence, fluorescence sensing, gas chromatography-mass spectrometer (GC-MS), etc. Normally, GC-MS is highly sensitive and responsive but rely on bulky, expensive instruments that make it difficult to meet the requirements of the simplicity of diagnosis and

* Corresponding author.
** Corresponding author.
E-mail addresses: gaoyixun@m.scnu.edu.cn (Y. Gao), wangyao@m.scnu.edu.cn (Y. Wang).

https://doi.org/10.1016/j.talanta.2024.127365
Received 2 July 2024; Received in revised form 2 December 2024; Accepted 8 December 2024
Available online 12 December 2024

treatment [11–13]. Based on fluorescence sensing, fluorescent probes with structures such as phenylamine and *o*-phenylenediamine possess superior sensitivity and selectivity toward NO at room temperature, but the complex synthesis processes and poor reversibility of response limit their practical application [14,15]. Recently, metal oxide semiconductors (MOS) such as ZnO [16], WO_3 [17], SnO_2 [18], etc., have become research hotspot of chemiresistive detection of NO gas. However, since the sensing process requires the involvement of oxygen species that has to be produced at high temperatures, the MOS-based sensors typically work at a relatively high operating temperatures (usually >100 °C), which leads to high energy consumption and fire hazards [19,20]. Above all, there is an urgent demand for room temperature chemiresistive NO sensors with high sensitivity, reversibility, and selectivity for practical applications.

Two-dimensional (2D) carbon-based materials such as graphene, graphitic carbon nitride (g-C_3N_4), MXene, etc., which are well known by their mild operating temperature, have drawn a wide attention in the field of gas sensing [21–24]. Researchers typically adopted functionalization approaches to overcome the poor sensitivity and selectivity of their intrinsic form [25–29]. In 2022, Wang et al. [30] reported that the composite of Hemin (Fe (III)-protoporphyrin IX) and graphene exhibited distinct performance for room temperature NO sensing depending on the specific interactions between iron and NO. Nevertheless, the self-stacking of porphyrin rings severely blocks iron ions from contact with NO molecules, resulting in its poor gas sensitivity. It could be deduced that constructing similar composites with graphene and iron-containing metal-organic small molecule with unoccupied active sites would achieve better room-temperature NO sensing performance.

Ferrocene, a metal-organic compound consisting of two cyclopentadiene and a ferrous ion (Fe^{2+}) with a sandwich structure, has been widely used as catalysts and modifier of functional materials [31–33]. As an iron-containing metal-organic small molecule, it possesses three advantages for graphene-based NO gas sensor. Firstly, as a mature developed reagent, ferrocene has relatively stable chemical and physical properties to be involved in gas sensing process. Secondly, the iron ion of ferrocene would not be obstructed by cyclopentadiene because of its sandwich structure, while the aromatic rings could also compose with graphene via π-π interaction. And last but not least, specific chemical reaction would occur between ferrocene and NO, which has been reported by Priya Sudhesh et al. [34] in 2016. Therefore, it is reasonable to hypothesize that assembling graphene with iron-contained ferrocene would construct a distinctive room temperature NO sensing material.

In this work, an assembly of ferrocene (Fc) and reduced graphene oxide (rGO) was employed to fabricate NO sensing material (defined as Fc/rGO). The obtained Fc/rGO was prepared via a two-step preparation process including the reduction of graphene oxide followed by the assembly of ferrocene with rGO. The sensor possessed superior NO sensing performance including high response, reliable repeatability and high selectivity against other exhaled gases. Moreover, the sensing mechanism of Fc/rGO was further investigated via control experiments, X-ray photoelectron spectroscopy (XPS) measurement and Density functional theory (DFT) calculation. This work provides an approach of anchoring iron ions on graphene for gas sensing via supramolecular method.

2. Experimental section

2.1. Reagents and materials

The high-purity flake graphite (325 mesh) was purchased from XianFeng NANO Co., Ltd. Concentrated sulfuric acid (H_2SO_4, 98 %), hydrogen peroxide (H_2O_2, 31 %), potassium permanganate ($KMnO_4$), anhydrous ethanol, nickelocene, and ferrocene were purchased from Shanghai Titanchem Co., Ltd. Ruthenocene was purchased from Beijing Innochem Science & Technology Co., Ltd. Ag–Pd interdigitated electrodes (IDEs) were purchased from Beijing Elite Tech Co., Ltd.

2.2. Preparation of graphene oxide (GO) and rGO

GO was obtained by a modified Hummers' method [30]. The concentration of GO was 5 mg/mL. The rGO was prepared by hydrothermal method. Specifically, 10 mg of GO and 12 mL of deionized water were sonicated for 10 min and stirred for 30 min to form a brown solution. The above solution was then transferred to a 25 mL stainless steel autoclave and kept at 120 °C for 9 h. The resulting dispersion was filtered with vacuum and washed twice with deionized water. Then rGO was obtained.

2.3. Synthesis of Fc/rGO

The Fc/rGO was synthesized via a one-step solvothermal process. Firstly, 10 mg of rGO and 30 mg of ferrocene were dispersed in a mixture of 4 mL of deionized water and 20 mL of anhydrous ethanol, after which the dispersion was sonicated for 10 min and stirred for 9 h. Secondly, the above dispersion was transferred to two 25 mL stainless steel autoclaves and kept at 120 °C for 5 h. The resulting dispersion was filtered with vacuum and washed twice with anhydrous ethanol. Finally, the dispersion was redispersed in 15 mL of anhydrous ethanol using ultrasonication. The optimum amount of ferrocene was discovered by controlled experiments as shown in Fig. 3b. During the preparation of Fc/rGO, the percentage of ethanol of the solvent mixture used for solvothermal and the amount of ferrocene added affected the NO sensing performance of Fc/rGO, so comparative experiments were carried out, and the experimental results are shown in Fig. S2.

2.4. Materials characterization

The morphology and elemental composition of the materials were observed by using a scan electron microscope (SEM, Quanta 250 FEG, FEI, America) and a transmission electron microscopy (TEM, Talos F200X, FEI) with energy dispersive X-ray spectroscopy mapping (EDS mapping). Surface chemical groups of materials were characterized by using Fourier transform infrared (FT-IR) spectrophotometer (Vertex 70, Bruker, Germany) using potassium bromide (KBr) plate method in a spectral range of 4000-400 cm^{-1} with the resolution of 2 cm^{-1}. Raman spectra were obtained by Raman microscope (inVia, RENISHAW, UK) at an excitation wavelength of 532 nm. Element compositions were obtained by XPS (Escalab 250Xi, Thermo Fisher, UK) with a mono X-ray source Al Kα as the incident radiation. The binding energy calibration was based on C 1s at 284.0 eV.

2.5. Gas sensing measurements

Keithley 2450 Sourcemeter was employed to obtain resistance values for sensing materials. IDEs should be ultrasonically cleaned with ethanol for 30 min before use. 10 μL of rGO or Fc/rGO dispersion was dropped onto the IDEs, after which the IDEs were dried in an oven at 65 °C for 5 min. The sensing test cycle contains three consecutive steps. Firstly, the IDEs were placed into a blank chamber filled with air (relative humidity: 20 %) to record the baseline. Secondly, after the baseline has stabilized, the IDEs were transferred to a sensing test chamber filled with a specific concentration of target gas (diluted with N_2). Thirdly, when the response curve leveled off, the IDEs were transferred to a blank chamber filled with dry air. All gas sensing measurements were performed at room temperature (25 ± 2 °C) [35].

2.6. DFT calculation

In the theoretical calculation, the B3LYP exchange-correlation function and Grimme's DFT-D3(BJ) empirical dispersion correction were employed for geometric optimizations [36]. The def2-TZVP basis set was employed for all elements. Gaussian was used for DFT calculations and Multiwfn was used for analysis [37].

3. Results and discussion

The synthesis process is illustrated in Scheme 1 rGO and ferrocene were assembled by a simple solvothermal method in a mixed solvent of ethanol and water, yielding a suspension liquid of Fc/rGO. Additionally, control experiments without the introduction of ferrocene were conducted to obtain rGO for comparison.

The Raman spectra of rGO and Fc/rGO exhibited the main characteristics of graphene-based materials. As Fig. 1a showed, two broad peaks at 1346 and 1603 cm^{-1} corresponded to the characteristic D- and G-bands of graphene, respectively [38]. The functional groups of ferrocene, rGO, and Fc/rGO were characterized by FT-IR respectively. As shown in Fig. 1b, in the FT-IR spectrum of the ferrocene, the peak at 484 cm^{-1} was attributed to the stretching vibration of the cyclopentadienyl ring and Ferrum in ferrocene [39]. In the FT-IR spectrum of the rGO, a broad peak at 3431 cm^{-1} was observed, which was attributed to the O–H stretching vibration. The peak at 1628 cm^{-1} was attributed to C–O bending vibrations [40]. In the FT-IR spectrum of the Fc/rGO, there is not only the O–H stretching vibration peak of rGO at 3428 cm^{-1} but also the cyclopentadienyl ring and Ferrum stretching vibration peak at 491 cm^{-1}, which indicates that ferrocene is successfully anchored on rGO.

XPS spectra of Fc/rGO were obtained and shown in Fig. 1c–f. The survey spectra sample verified the existence of carbon, oxygen, and iron. Firstly, the high-resolution spectra of C 1s of Fc/rGO are shown in Fig. 1d. Three peaks centered at 288.18, 285.47, and 284.00 eV were attributed to C═O, C–O, and C–C bonds respectively. Secondly, in Fig. 1e, the high-resolution spectra of the O 1s of Fc/rGO revealed the peaks at 532.97 and 531.62 eV, assigned to C═O and C–O bonds respectively. Thirdly, the peaks of the Fe $2p_{3/2}$ band (710.07 eV) and Fe $2p_{1/2}$ band (724.11 eV) were presented in the high-resolution spectra of Fe 2p of Fc/rGO [41,42]. The appearance of iron in XPS spectra of Fc/rGO proved that the composite material was successfully prepared as expected.

TEM and SEM images were obtained to observe the morphology and structure of the materials. As displayed in Fig. 2a, smooth graphene nanosheets were discovered in the SEM images of rGO, while rough surface was observed from Fc/rGO after the introduction of ferrocene. Besides, as shown in Fig. S1, iron atoms were found in the EDS of Fc/rGO but not in rGO, which proves the success of the combination of ferrocene.

Furthermore, as shown in Fig. 2, muslin-like graphene nanosheets were discovered in the TEM images of rGO, and the aggregates in the TEM of Fc/rGO indicate the successful assembly of ferrocene and rGO. To further demonstrate the presence of ferrocene in the composite, the high-angle annular dark-field scanning transmission electron microscopy (HAADF-STEM) was employed and the corresponding EDS elemental mapping images were obtained to observe the elemental composition of the Fc/rGO. As shown in Fig. 2. The elemental mapping characterization demonstrated that the C, O, and Fe elements were uniformly distributed on the composite. The uniform distribution indicates the successful preparation of the Fc/rGO composite.

In order to explore the sensing performance of ferrocene assembled graphene, the sensors were fabricated on IDEs with rGO and Fc/rGO as sensing materials. The gas sensing tests were conducted at 25 °C for NO (N_2 as background). The detailed data of resistance value was listed in Table S1.

As shown in Fig. 3a, the response of the Fc/rGO sensor to 1 ppm NO gas was noticeably enhanced ($R_a/R_g = 1.73$) compared to rGO. The T_{res} and T_{rec} of Fc/rGO toward 1 ppm NO were 364 s and 1760 s, respectively. Here, T_{res} was defined as the time needed to reach 90 % of the maximum response, while T_{rec} was defined as the time for the resistance in equilibrium to go down to 10 % of the initial value after releasing the test gas. Furthermore, the optimum amount of ferrocene was explored (Fig. 3b). With the increase of ferrocene dosage, the response of the composites to 1 ppm NO firstly increased and then remained at a close level with a slight decrease. This result was mainly because the introduced ferrocene gradually reached saturation, while the excessive ferrocene was washed away. Therefore, 30 mg of ferrocene introduction was was determined as the optimal condition to prepare materials for subsequent experiments. In addition, Fig. 3c and **d** showed excellent linearity between gas concentration (0.2–8 ppm) and response values, as well as reliable sensing repeatability for NO at room temperature. The gradual increase in baseline could be ascribed to the slower diffusion of NO after multiple cycles.

Typically, there is a high demand for the stability and selectivity of gas sensors in practical applications of clinical diagnostics. An aging experiment of the Fc/rGO sensor was performed for over 40 days (Fig. 3e). The response of the Fc/rGO sensor remained around 96 % of the initial value after 40 days, which indicated the excellent stability of the composite. As for the selectivity, as displayed in Fig. 3f, the Fc/rGO sensor possessed a much higher response toward NO ($R_a/R_g = 1.73$, 1 ppm) than other exhaled gases including ammonia ($R_a/R_g = 0.96$, 10 ppm), acetone ($R_a/R_g = 0.97$, 100 ppm), ethanol ($R_a/R_g = 0.98$, 100 ppm), methanol ($R_a/R_g = 0.99$, 100 ppm) and BTEX (a mixture of benzene, toluene, ethylbenzene, and xylene, $R_a/R_g = 1.01$, 10 ppm). The excellent selectivity of Fc/rGO for NO could be attributed to the specific interaction between ferrocene and NO molecules. It is worth mentioned that humidity resistance is an important factor for gas sensors, especially for exhaled gas. As shown in Fig. S3, the response values of Fc/rGO under 0–75 % relative humidity were 1.73, 1.45, 1.33, and 1.04, respectively. The possible reason might be that water molecules would occupy the reactive sites on the central Fe ions in ferrocene, which is similar to the case of metalloporphyrin as early reported [30]. Drying devices that have already been developed in modern exhaled breath testing could be applied to solve this problem [43].

For comparison, Table 1 summarized all the reported carbon-based room temperature NO gas sensors, indicating that the gas sensing performance of Fc/rGO was in a leading position. The Fc/rGO-based sensor possessed excellent response and a practical LOD of 200 ppb, which is relatively low for NO under RT conditions for carbon-based sensitive materials.

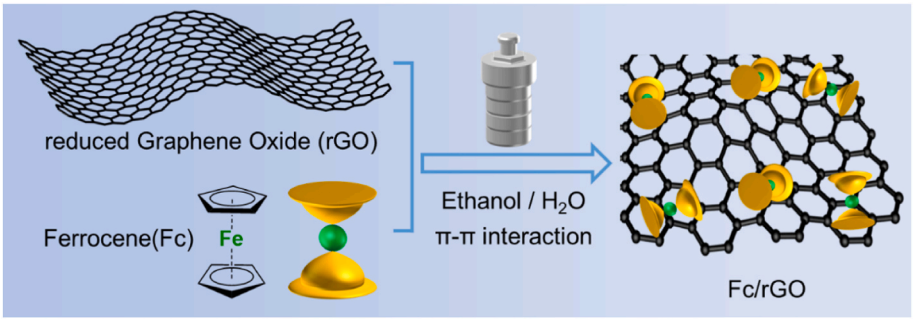

Scheme 1. The preparation process of ferrocene and reduced graphene oxide composite Fc/rGO.

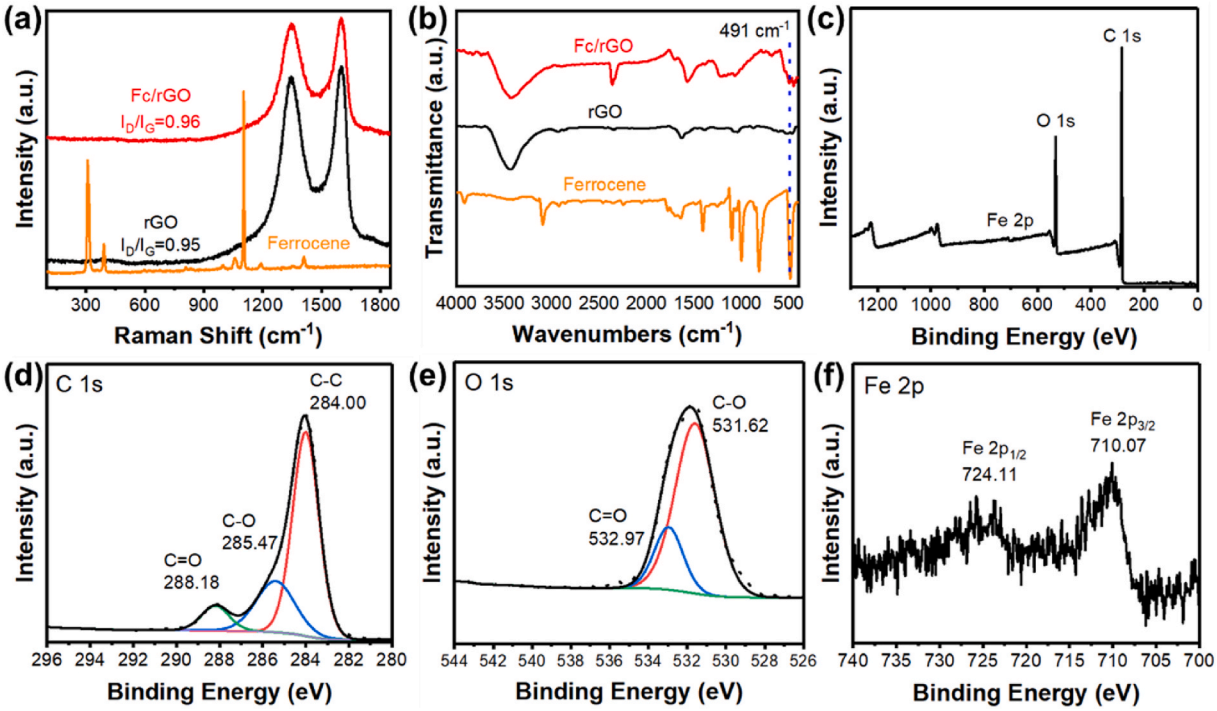

Fig. 1. (a) Raman spectra and (b) FT-IR spectra of ferrocene, rGO, and Fc/rGO materials; XPS spectra of Fc/rGO: Survey spectra of (c) Fc/rGO; high-resolution spectra of C 1s (d), O 1s (e), and Fe 2p (f) of Fc/rGO.

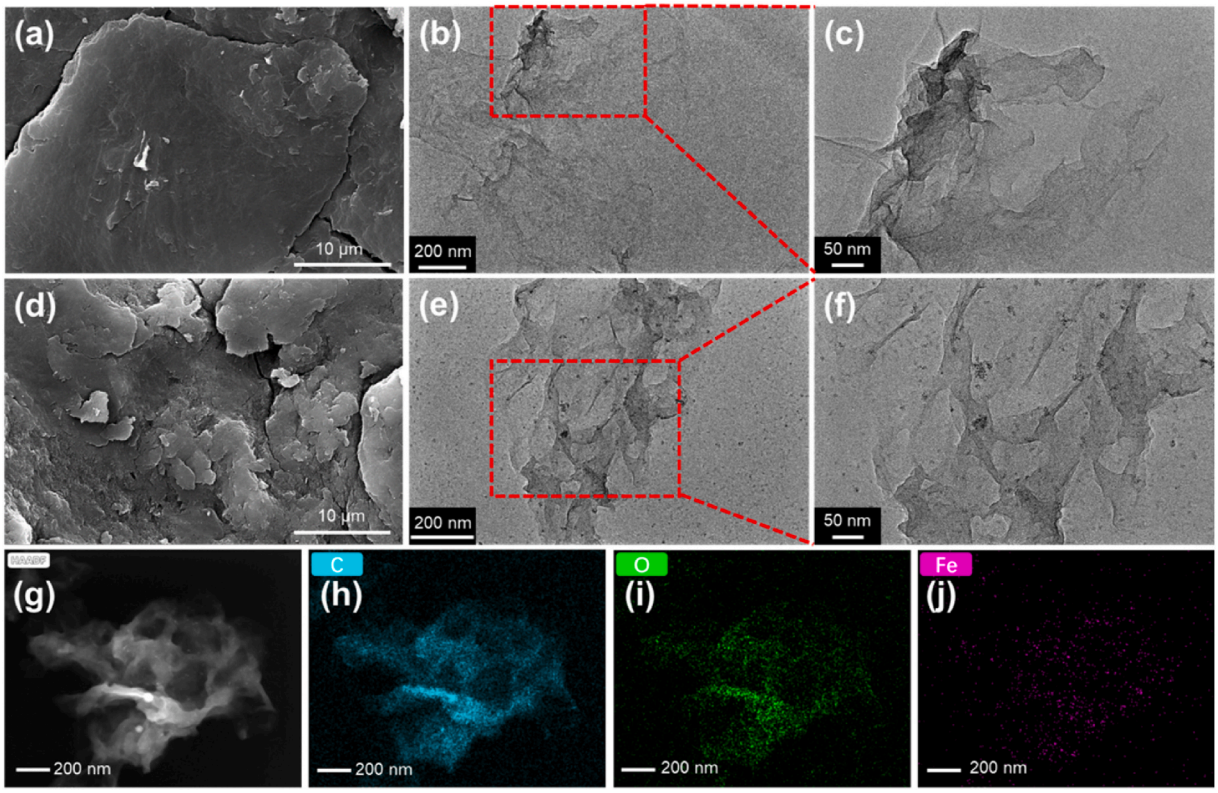

Fig. 2. SEM images of (a) rGO and (d) Fc/rGO. TEM images of (b, c) rGO and (e, f) Fc/rGO. HAADF-STEM (g) and EDS elemental mapping images of C (h), O (i), and Fe (j) of Fc/rGO.

3.1. Gas sensing mechanism

To further explore the significance of iron in NO gas-sensing, as shown in Fig. 4a, ferrocene was changed into nickelocene (Nc) and ruthenocene (Rc) for control experiments. The corresponding control groups were named as Nc/rGO and Rc/rGO, respectively. EDS and XPS

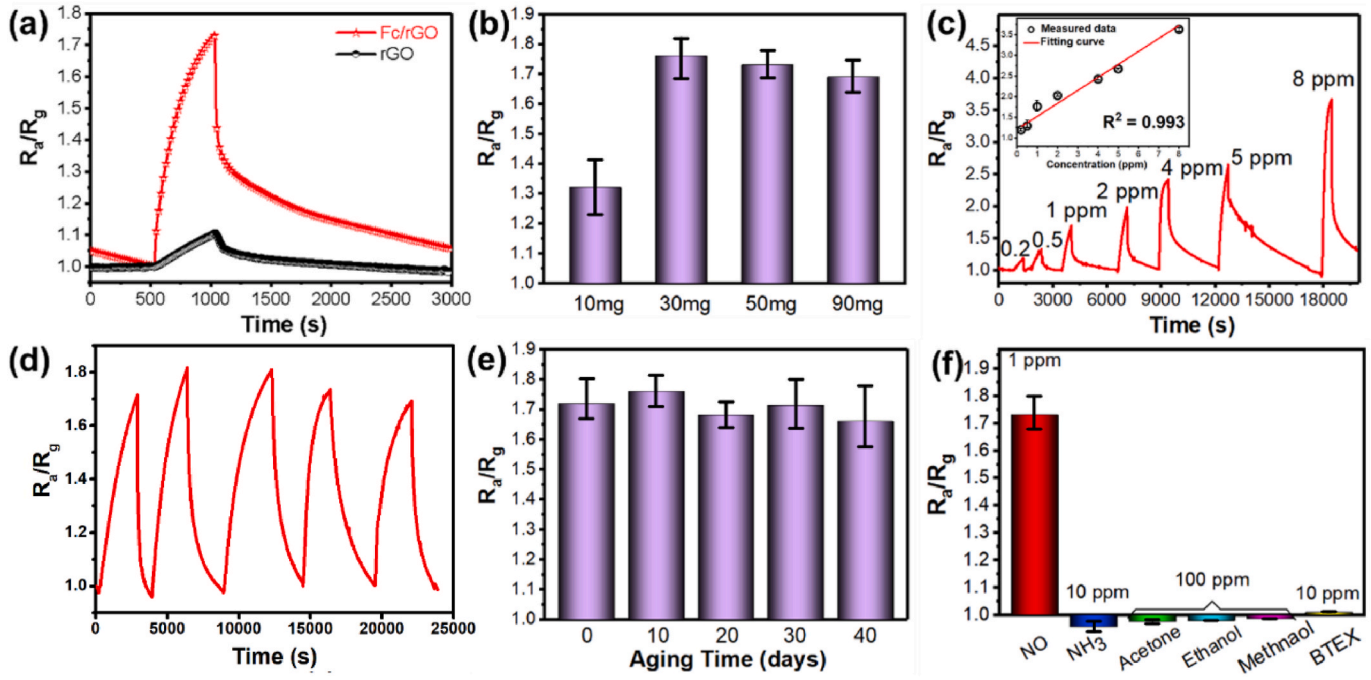

Fig. 3. (a) Response-recovery curves of rGO (black) and Fc/rGO (red) sensors toward 1 ppm of NO. (b) Response values of Fc/rGO after the introduction of different amounts of ferrocene. (c) Consecutive response-recovery curve of Fc/rGO sensors toward various NO concentrations from 0.2 to 8 ppm. Inset: corresponding linear fit of the responses of NO concentration (R-square = 0.993). Error bars for the data points lie within the symbols themselves. (d) Cyclic response curve of Fc/rGO sensors upon exposure to 1 ppm NO. (e) Aging test Fc/rGO sensors toward 1 ppm of NO for 40 days. (f) Selective response of the Fc/rGO sensors toward NO and interferential gases including NH_3, acetone, ethanol, methanol, and BTEX. (For interpretation of the references to colour in this figure legend, the reader is referred to the Web version of this article.)

Table 1
Comparison of NO sensing properties of carbon-based materials at room temperature.

Materials	NO (ppm)	Response[a]	T_{res}/T_{rec}[b] (s/s)	D_R[c] (ppm)	pLOD[d] (ppm)
TiO_2@NGQDs[e] [44]	100	0.76	235/285	10–100	10
MoS_2/rGO/paper [45]	2	1.06	150/ >600	2–10	2
CNFs/CoS_2/MoS_2 [46]	10	≈1.045	1200/ 6000	1–100	1
SWNT@MoS_2 [47]	100	1.18	45/528	1–300	1
TiO_2/rGO [48]	2.75	1.06	440/881	0.69–2.75	0.69
Hemin-N-rGO [30]	1	1.34	229/770	0.5–20	0.5
N-rGO [49]	1	1.7	≈100/–	0.4–1	0.4
SWCNT@PEI [50]	1	≈2.5	≈1800/ >3000	0.1–5	0.1
en-APTAS@SWCNTs [51]	2	1.37	≈600/ >600	–	0.1
HNS-rGO [40]	1	<1.5	≈261/ ≈500	0.1–20	0.1
Fc/rGO (This work)	1	1.73	364/ 1760	0.2–8	0.2

[a] Response is defined as Response = R_a/R_g (R_a denotes the resistance the material in N_2 and R_g denotes the resistance the material in the target gas).
[b] T_{res} and T_{rec} represent the response time and recovery time.
[c] D_R represents the detection range.
[d] pLOD represents practical limit of detection.
[e] The gas sensing performance of TiO_2@NGQDs was carried out under 365 nm illumination.

measurements were carried out to confirm the successful preparation of the composites Nc/rGO and Rc/rGO (Figs. S5 and S6). NO sensing tests of these two control groups were then carried out, as shown in Fig. 4b and c. Compared with Fc/rGO, the response value of Rc/rGO to 1 ppm NO was 1.33, while Nc/rGO performed no significant response, indicating that iron plays a key role in the sensing process.

In addition, XPS measurements were carried out to reveal the sensing process. For pretreatment, Fc/rGO and pristine rGO were respectively sealed in excess NO gas (500 ppm, N_2 as background) for 3 days. Subsequently, XPS spectra of these two samples and the control groups without NO treatment were obtained.

As shown in Fig. 5a, there was no obvious difference in the N 1s band of rGO before and after NO treatment. However, as shown in Fig. 5b, the N 1s band of Fc/rGO showed a significant peak after NO treatment. Moreover, the NO adsorption peak was found at 530.35 eV in the corresponding high-resolution XPS spectra of O 1s (Fig. 5c) [34,52]. Therefore, it could be speculated that the assembly of ferrocene would enhance the adsorption capacity of the material for NO, resulting in excellent sensing properties. As shown in Fig. 5d, the peak of Fe $2p_{3/2}$ blue shifted from 710.07 eV to 710.62 eV after NO treatment. This variation in binding energy was thought to be the result of electron transfer from Fc/rGO to NO gas molecules when gas molecules were adsorbed onto the surface of the assembly [53].

At last, theoretical analysis was carried out to investigate the inner sensing mechanism. In 2019 Salma et al. [54] demonstrated by DFT calculation that the ferrocene molecules would be composited with graphene in such a way that their molecular axes are parallel to the plane of graphene through. This edge-to-face configuration possesses higher adsorption energy, lower system energy, and higher stability than the face-to-face configuration. Specifically, based on the principle of π-π interactions, it can be hypothesized that the edge-to-face configuration would result in weak electrostatic interaction between the slightly electron-deficient hydrogen atoms on cyclopentadiene and the electron-rich graphene [55,56]. To further prove the above speculations, the possible configurations of ferrocene with rGO were simulated by DFT. As shown in Fig. 6, after geometry optimization, the DFT simulation showed that the total energy of the face-to-face configuration was −10.7518 kcal/mol, while the total energy of the edge-to-face

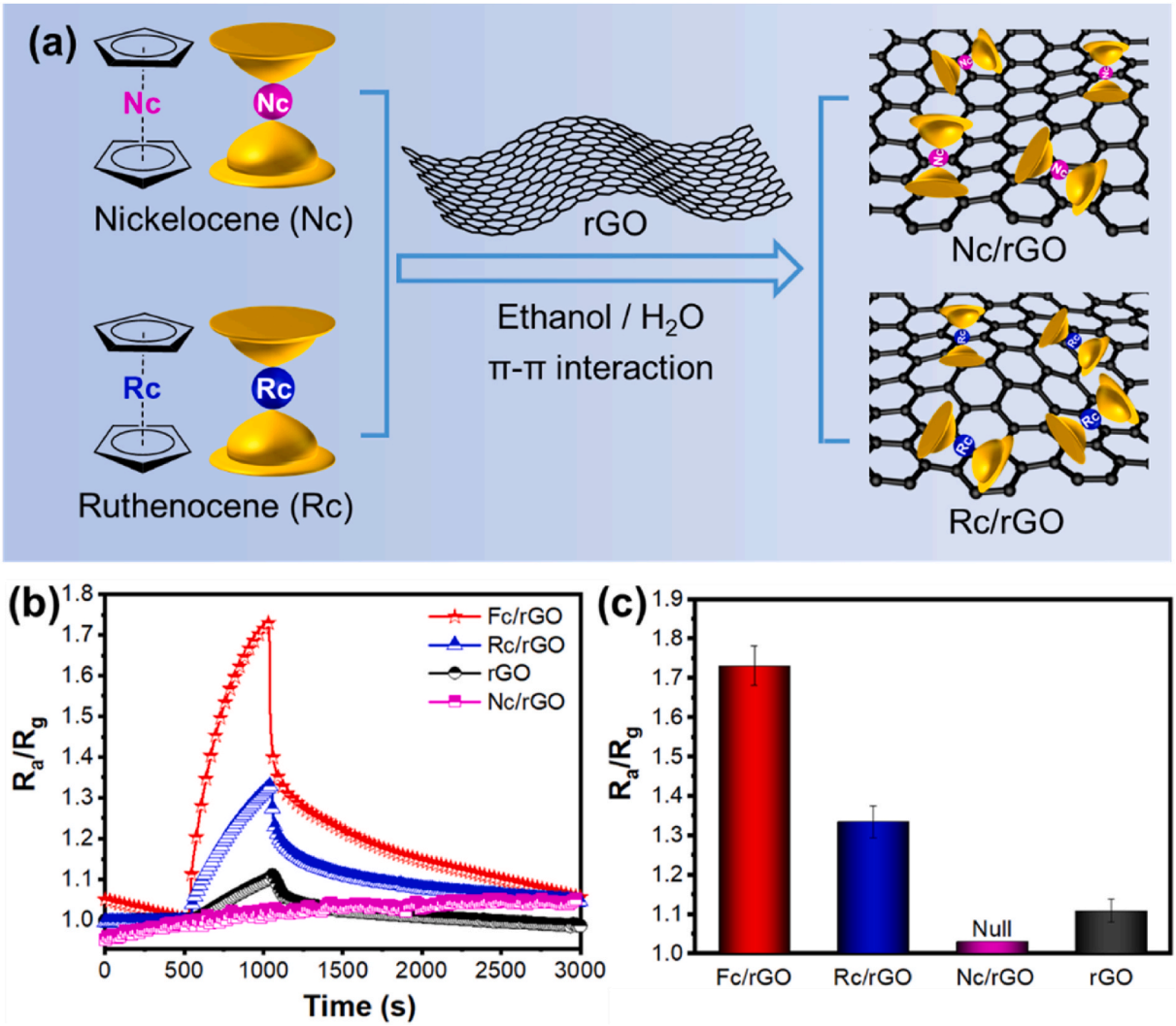

Fig. 4. (a) Synthesis of Nc/rGO and Rc/rGO composites of nickelocene and ruthenocene with reduced graphene oxide. (b, c) Response toward 1 ppm NO gas of Fc/rGO (i), Rc/rGO (ii), rGO (iii), and Nc/rGO (iv).

configuration was lower (−11.9854 kcal/mol), It could be deduced from the results that the supramolecular assembling of Fc/rGO was controlled by the π-π stacking interaction between graphene and ferrocene, taking the configuration energy as consideration [57]. Two cyclopentadiene rings involved in the interaction with graphene rather than one, which would be the possible reason that the edge-to-face configuration has lower total energy than face-to-face.

Independent gradient model based on Hirshfeld partition (IGMH) analysis was carried out to further visualize the interaction inside the Fc/rGO [58]. As revealed in Fig. 6c, obvious interaction between ferrocene and graphene was present in the Fc/rGO assembly, indicating that more electrons would accumulate at the lower part of the ferrocene and the surface of the graphene sheet. This configuration would facilitate the constructing of effective charge transport channel between ferrocene and graphene [59]. Besides, by comparison with a typical reducing gas, ammonia, it is clear that NO act as electron-withdrawing molecules in the sensing process (Fig. 3f). Therefore, the direction of charge transfer was from graphene to the ferrocene molecules.

These results suggested that ferrocene plays a key role in NO sensing by enhancing adsorption capacity and electron transfer. Bicyclopentadiene would act as a container for the Fe^{2+} to be anchored onto the surface of graphene to better utilize the sensing properties in NO sensing. The sensing mechanism based on charge transfer was proposed as shown in Scheme 2 and **Equations (1)–(4)**(Ferrocene is expressed as $(C_5H_6)_2Fe^{2+}$).

$$rGO\text{-}(C_5H_6)_2Fe^{2+} + NO \rightarrow rGO\text{-}(C_5H_6)_2Fe^{2+}(NO) \quad (1)$$

$$rGO\text{-}(C_5H_6)_2Fe^{2+}(NO) \rightarrow rGO\text{-}(C_5H_6)_2Fe^{3+}(NO)^{-} \quad (2)$$

$$rGO\text{-}(C_5H_6)_2Fe^{3+}(NO)^{-} \rightarrow (rGO)^{+}\text{-}(C_5H_6)_2Fe^{2+}(NO)^{-} \quad (3)$$

$$(rGO)^{+}\text{-}(C_5H_6)_2Fe^{2+}(NO)^{-} \rightarrow rGO\text{-}(C_5H_6)_2Fe^{2+} + NO \quad (4)$$

(1) NO molecules were adsorbed onto the surface of the assembly and came into contact with Fe ions. (2) Electrons were transferred from the graphene to the Fe ions and subsequently to NO molecules, which possess strong electronegativity. (3) As a result, the hole concentration of rGO increases with the increasing NO concentration, leading to a decrease in the resistance of the sensing material. (4) Finally, the resistance of Fc/rGO would recover to its initial value by the removing NO from the sensing system, accompany with the return of the electron to graphene.

4. Conclusion

We successfully prepared a composite (Fc/rGO) of rGO and ferrocene by one-step solvothermal method. The introduction of ferrocene enhances the adsorption capacity of the material for NO, resulting in excellent gas-sensitive properties. Benefiting from the introduction of

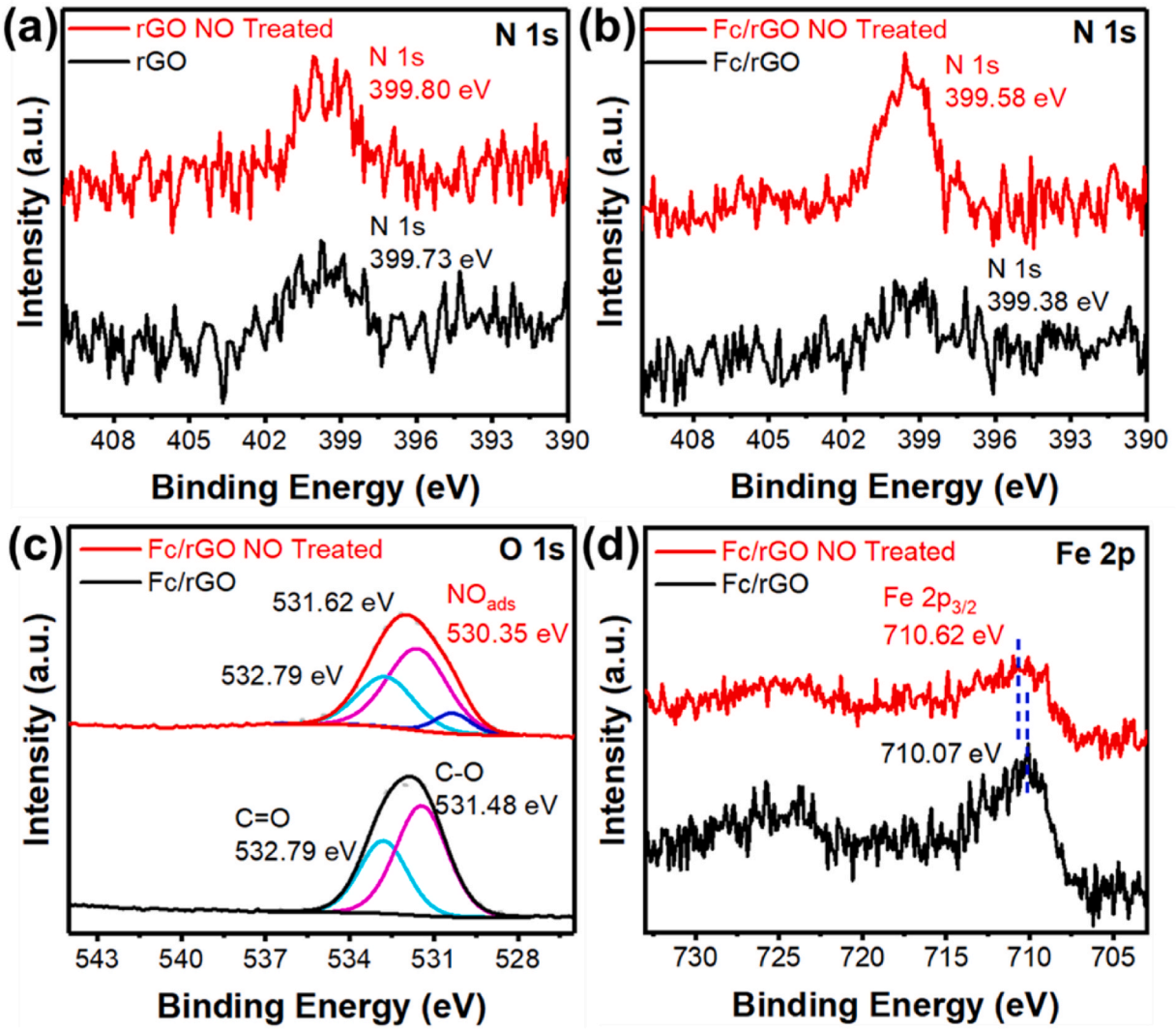

Fig. 5. High-resolution XPS spectra of N 1s of a) rGO and b) Fc/rGO; c) High-resolution XPS spectra of O 1s of Fc/rGO; d) High-resolution XPS spectra of Fe 2p of Fc/rGO (The red line represents material treated with NO, the black line represents material not treated with NO). (For interpretation of the references to colour in this figure legend, the reader is referred to the Web version of this article.)

ferrocene, the Fc/rGO possessed superior sensing performance (R_a/R_g = 1.73, 1 ppm NO, response time <400 s) with a practical LOD of 200 ppb, reliable repeatability (over 7 cycles), excellent selectivity against other exhaled gases, and high stability (less than 4 % decrease over 40 days). It is also explored that the excellent performance of NO gas-sensitive performance is mainly attributed to the introduction of ferrocene to enhance the adsorption capacity of Fc/rGO for NO, in which ferrous ions play a role in NO adsorption as well as electron transport. This work not only provides guidance for the utilization of ferrocene-containing compounds for NO sensing, but also opens the way for the preparation of Fe/C composites.

CRediT authorship contribution statement

Lulu Zhang: Writing – original draft, Investigation, Formal analysis, Data curation. **Yixun Gao:** Writing – review & editing, Methodology, Funding acquisition, Conceptualization. **Yancong Feng:** Visualization, Software. **Zhijian Mai:** Visualization, Software. **Jianqiang Wang:** Methodology. **Yanwei Chang:** Visualization. **Fengnan Wang:** Validation. **Hao Li:** Resources, Project administration. **Peerasak Paoprasert:** Resources. **Yi-Kuen Lee:** Resources. **Paddy J. French:** Resources. **Ahmad M. Umar Siddiqui:** Resources. **Guofu Zhou:** Resources, Project administration. **Yao Wang:** Writing – review & editing, Supervision, Project administration, Methodology, Funding acquisition.

Declaration of competing interest

The authors declare the following financial interests/personal relationships which may be considered as potential competing interests: Yao Wang reports financial support was provided by National Natural Science Foundation of China. Yao Wang reports financial support was provided by Science and Technology Program of Guangzhou. Yao Wang reports financial support was provided by Guangdong Basic and Applied Basic Research Foundation. Yixun Gao reports financial support was provided by Guangdong Basic and Applied Basic Research Foundation. Yao Wang reports financial support was provided by Innovative Team Project of Education Bureau of Guangdong Province. Yao Wang reports financial support was provided by Guangdong Science and Technology Project-International Cooperation. Yao Wang reports financial support was provided by Startup Foundation from SCNU. Yao Wang reports financial support was provided by Guangdong Provincial Key Laboratory of Optical Information Materials and Technology. Yao Wang reports financial support was provided by MOE International Laboratory for Optical Information Technologies. Yao Wang reports financial support

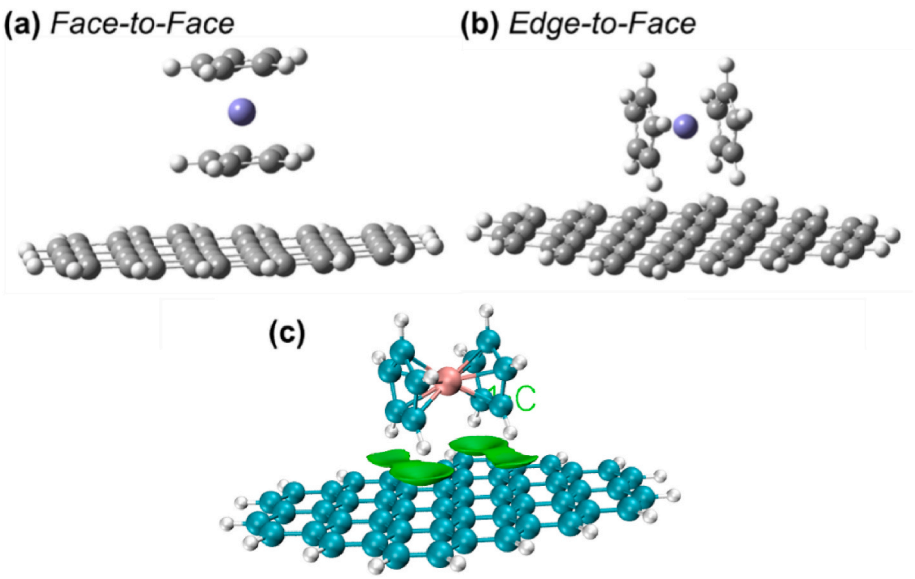

Fig. 6. Orientation scheme for the adsorption of ferrocene on graphene substrate. a) Face-to-face configuration; b) Edge-to-face configuration; c) Independent gradient model based on Hirshfeld partition (IGMH) analysis of Fc/rGO. Green regions indicate the interaction between ferrocene and graphene. (For interpretation of the references to colour in this figure legend, the reader is referred to the Web version of this article.)

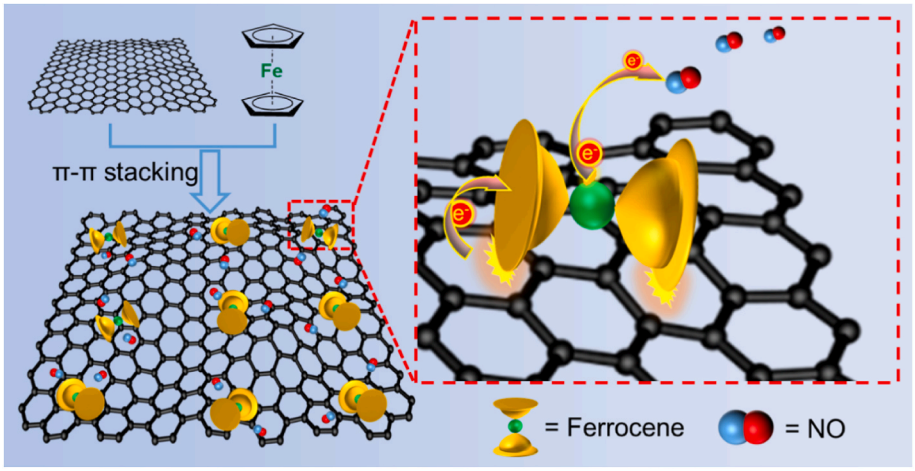

Scheme 2. Schematic diagram of the sensing mechanism of Fc/rGO for NO.

was provided by the 111 Project. Yao Wang reports financial support was provided by High-end Foreign Experts Recruitment Program. If there are other authors, they declare that they have no known competing financial interests or personal relationships that could have appeared to influence the work reported in this paper.

Acknowledgments

This work was supported by the National Natural Science Foundation of China (Grant No. 51973070), Science and Technology Program of Guangzhou (No. 2019050001), Guangdong Basic and Applied Basic Research Foundation (2022A1515010577, 2023A1515010814), Innovative Team Project of Education Bureau of Guangdong Province (2018KCXTD009), Guangdong Science and Technology Project-International Cooperation (2022A0505050069), Startup Foundation from SCNU, Guangdong Provincial Key Laboratory of Optical Information Materials and Technology (2023B1212060065), MOE International Laboratory for Optical Information Technologies, the 111 Project, High-end Foreign Experts Recruitment Program (DL2023030001L).

Appendix A. Supplementary data

Supplementary data to this article can be found online at https://doi.org/10.1016/j.talanta.2024.127365.

Data availability

Data will be made available on request.

References

[1] G. Kumar, S.K. Dey, S. Kundu, Functional implications of vascular endothelium in regulation of endothelial nitric oxide synthesis to control blood pressure and cardiac functions, Life Sci. 259 (2020) 118377, https://doi.org/10.1016/j.lfs.2020.118377.

[2] V. Calabrese, C. Mancuso, M. Calvani, E. Rizzarelli, D.A. Butterfield, A.M. Giuffrida Stella, Nitric oxide in the central nervous system: neuroprotection versus neurotoxicity, Nat. Rev. Neurosci. 8 (2007) 766–775, https://doi.org/10.1038/nrn2214.

[3] M.D. Brown, M.H. Schoenfisch, Electrochemical nitric oxide sensors: principles of design and characterization, Chem. Rev. 119 (2019) 11551–11575, https://doi.org/10.1021/acs.chemrev.8b00797.

[4] Y. Yang, Z. Huang, L. Li, Advanced nitric oxide donors: chemical structure of NO drugs, NO nanomedicines and biomedical applications, Nanoscale 13 (2021) 444–459, https://doi.org/10.1039/d0nr07484e.

[5] B. Yin, Y. Guo, Y. Liu, Y. Zhao, S. Huang, X. Wei, H. Wang, R. Liu, Y. Liu, Y. Tang, Molecular mechanism of Chuanxiong Rhizoma in treating coronary artery diseases, Chin. Herb. Med. 13 (2021) 396–402, https://doi.org/10.1016/j.chmed.2021.03.001.

[6] A. Vasilescu, B. Hrinczenko, G.M. Swain, S.F. Peteu, Exhaled breath biomarker sensing, Biosens. Bioelectron. 182 (2021) 113193, https://doi.org/10.1016/j.bios.2021.113193.

[7] L.E. Gustafsson, A.M. Leone, M.G. Persson, N.P. Wiklund, S. Moncada, Endogenous nitric oxide is present in the exhaled air of rabbits, Guinea pigs and humans, Biochem. Biophys. Res. Commun. 2 (1991) 852–857, https://doi.org/10.1016/0006-291x(91)91268-h.

[8] B.J. Privett, J.H. Shin, M.H. Schoenfisch, Electrochemical nitric oxide sensors for physiological measurements, Chem. Soc. Rev. 39 (2010) 1925–1935, https://doi.org/10.1039/b701906h.

[9] M. Król, M. Kepinska, Human nitric oxide synthase-its functions, polymorphisms, and inhibitors in the context of inflammation, diabetes and cardiovascular diseases, Int. J. Mol. Sci. 22 (2021) 56, https://doi.org/10.3390/ijms22010056.

[10] E. Goshi, G. Zhou, Q. He, Nitric oxide detection methods in vitro and in vivo, Med. Gas Res. 9 (2019) 192, https://doi.org/10.4103/2045-9912.273957.

[11] A. Sharma, R. Kumar, P. Varadwaj, Smelling the disease: diagnostic potential of breath analysis, Mol. Diagn. Ther. 27 (2023) 321–347, https://doi.org/10.1007/s40291-023-00640-7.

[12] J.N. Bates, Nitric oxide measurement by chemiluminescence detection, Neuroprotocols 1 (1992) 141–149, https://doi.org/10.1016/1058-6741(92)90045-y.

[13] P.J. Kipping, P.G. Jeffery, Detection of nitric oxide by gas chromatography, Nature 200 (1963) 1314, https://doi.org/10.1038/2001314a0.

[14] X. Chen, L. Niu, Q. Yang, Visualizing the underlying signaling pathway related to nitric oxide and glutathione in cardiovascular disease therapy by a sequentially activated fluorescent probe, Anal. Chem. 93 (2021) 3922–3928, https://doi.org/10.1021/acs.analchem.0c04754.

[15] W. Jiang, Y. Li, H. Liu, D. Zhou, J. Ou-Yang, L. Yi, C. Li, A rhodamine-deoxylactam based fluorescent probe for fast and selective detection of nitric oxide in living cells, Talanta 197 (2019) 436–443, https://doi.org/10.1016/j.talanta.2019.01.061.

[16] C. Li, B. Song, M. Lv, G. Chen, X. Zhang, Z. Deng, Y. Xu, L. Huo, S. Gao, Highly sensitive and selective nitric oxide sensor based on biomorphic ZnO microtubes with dual-defects assistance at low temperature, Chem. Eng. J. 446 (2022) 136846, https://doi.org/10.1016/j.cej.2022.136846.

[17] Z. Cai, H. Li, J. Ding, X. Guo, Hierarchical flowerlike WO_3 nanostructures assembled by porous nanoflakes for enhanced NO gas sensing, Sensor. Actuator. B Chem. 246 (2017) 225–234, https://doi.org/10.1016/j.snb.2017.02.075.

[18] B. Song, C. Li, X. Zhang, R. Gao, X. Cheng, Z. Deng, Y. Xu, L. Huo, S. Gao, A highly sensitive and selective nitric oxide/butanone temperature-dependent sensor based on waste biomass-derived mesoporous SnO_2 hierarchical microtubes, J. Mater. Chem. A 10 (2022) 14411–14422, https://doi.org/10.1039/d2ta03299f.

[19] Z. Ma, K. Yang, C. Xiao, L. Jia, Electrospun Bi-doped SnO_2 porous nanosheets for highly sensitive nitric oxide detection, J. Hazard Mater. 416 (2021) 126118, https://doi.org/10.1016/j.jhazmat.2021.126118.

[20] J. Li, M. Yang, X. Cheng, X. Zhang, C. Guo, Y. Xu, S. Gao, Z. Major, H. Zhao, L. Huo, Fast detection of NO_2 by porous SnO_2 nanotoast sensor at low temperature, J. Hazard Mater. 419 (2021) 126414, https://doi.org/10.1016/j.jhazmat.2021.126414.

[21] Z. Chen, J. Wang, D. Pan, Y. Wang, R. Noetzel, H. Li, P. Xie, W. Pei, A. Umar, L. Jiang, N. Li, N.F.D. Rooij, G. Zhou, Mimicking a dog's nose: scrolling graphene nanosheets, ACS Nano 12 (2018) 2521–2530, https://doi.org/10.1021/acsnano.7b08294.

[22] F. Schedin, A.K. Geim, S.V. Morozov, E.W. Hill, P. Blake, M.I. Katsnelson, K. S. Novoselov, Detection of individual gas molecules adsorbed on graphene, Nat. Mater. 6 (2007) 652–655, https://doi.org/10.1038/nmat1967.

[23] W. Pei, T. Zhang, Y. Wang, Z. Chen, A. Umar, H. Li, W. Guo, Enhancement of charge transfer between graphene and donor-π-acceptor molecule for ultrahigh sensing performance, Nanoscale 9 (2017) 16273–16280, https://doi.org/10.1039/c7nr04209d.

[24] W. Meng, S. Wu, X. Wang, D. Zhang, High-sensitivity resistive humidity sensor based on graphitic carbon nitride nanosheets and its application, Sensor. Actuator. B Chem. 315 (2020) 128058, https://doi.org/10.1016/j.snb.2020.128058.

[25] H. Zhang, X. Zhang, C. Qiu, P. Jia, F. An, L. Zhou, L. Zhu, D. Zhang, Polyaniline/ZnO heterostructure-based ammonia sensor self-powered by electrospinning of PTFE-PVDF/MXene piezo-tribo hybrid nanogenerator, Chem. Eng. J. 496 (2024) 154226, https://doi.org/10.1016/j.cej.2024.154226.

[26] Q. Feng, B. Huang, X. Li, Graphene-based heterostructure composite sensing materials for detection of nitrogen-containing harmful gases, Adv. Funct. Mater. 31 (2021) 2104058, https://doi.org/10.1002/adfm.202104058.

[27] J. Casanova-Chafer, P. Umek, S. Acosta, C. Bittencourt, E. Llobet, Graphene loading with polypyrrole nanoparticles for trace-level detection of ammonia at room temperature, ACS Appl. Mater. Interfaces 13 (2021) 40909–40921, https://doi.org/10.1021/acsami.1c10559.

[28] H. Hu, H. Liang, J. Fan, L. Guo, H. Li, N.F. de Rooij, A. Umar, H. Algarni, Y. Wang, G. Zhou, Assembling hollow cactus-like ZnO nanorods with dipole-modified graphene nanosheets for practical room-temperature formaldehyde sensing, ACS Appl. Mater. Interfaces 14 (2022) 13186–13195, https://doi.org/10.1021/acsami.1c20680.

[29] Y. Chang, J. Zhang, R. Lu, W. Li, Y. Feng, Y. Gao, H. Yang, F. Wang, H. Li, Y.K. Lee, P.J. French, A.M. Umar, Y. Wang, G. Zhou, Sheet-on-sheet architectural assembly of MOF/graphene for high-stability NO sensing at room temperature, J. Mater. Chem. C 12 (2024) 6966, https://doi.org/10.1039/d4tc00091a.

[30] Y. Gao, J. Wang, Y. Feng, N. Cao, H. Li, N.F. Rooij, A. Umar, P.J. French, Y. Wang, G. Zhou, CarbonIron electron transport channels in porphyrin-graphene complex for ppb-level room temperature NO gas sensing, Small 18 (2022) 2103259, https://doi.org/10.1002/smll.202103259.

[31] E. Matysiak-Brynda, J.P. Sęk, A. Kasprzak, A. Królikowska, M. Donten, M. Patrzalek, M. Poplawska, A.M. Nowicka, Reduced graphene oxide doping with nanometer-sized ferrocene moieties - new active material for glucose redox sensors, Biosens. Bioelectron. 128 (2019) 23–31, https://doi.org/10.1016/j.bios.2018.12.037.

[32] S. Priya, S. Berchmans, Ferrocene probe-assisted fluorescence quenching of PEI-carbon dots for NO detection and the logic gates based sensing of NO enabled by trimodal detection, Sci. Rep. 14 (2024) 10402, https://doi.org/10.1038/s41598-024-61117-z.

[33] Y. Xu, A. Stanko, C. Cerione, T. Lohrey, E. McLeod, B. Stoltz, J. Su, Low part-per-trillion, humidity resistant detection of nitric oxide using microtoroid optical resonators, ACS Appl. Mater. Interfaces 16 (2024) 5120–5128, https://doi.org/10.1021/acsami.3c16012.

[34] P. Sudhesh, T. Balamurugan, S. Berchmans, Insights into ferrocene-mediated nitric oxide sensing - elucidation of mechanism and isolation of intermediate, Electrochim. Acta 210 (2016) 321–327, https://doi.org/10.1016/j.electacta.2016.05.153.

[35] Y. Chang, M. Chen, Z. Fu, R. Lu, Y. Gao, F. Chen, H. Li, N. Frans De Rooij, Y. Lee, Y. Wang, G. Zhou, Building porphyrin-based MOFs on MXenes for ppb-level NO sensing, J. Mater. Chem. A 11 (2023) 6966–6977, https://doi.org/10.1039/d3ta00072a.

[36] L. Goerigk, S. Grimme, Efficient and accurate double-hybrid-meta-GGA density functionals-evaluation with the extended GMTKN30 database for general main group thermochemistry, kinetics, and noncovalent interactions, J. Chem. Theor. Comput. 7 (2011) 291–309, https://doi.org/10.1021/ct100466k.

[37] T. Lu, F. Chen, Multiwfn: a multifunctional wavefunction analyzer, J. Comput. Chem. 33 (2012) 580–592, https://doi.org/10.1002/jcc.22885.

[38] T.T. Tung, J. Yoo, F.K. Alotaibi, M.J. Nine, R. Karunagaran, M. Krebsz, G. T. Nguyen, D.N.H. Tran, J. Feller, D. Losic, Graphene oxide-assisted liquid phase exfoliation of graphite into graphene for highly conductive film and electromechanical sensors, ACS Appl. Mater. Interfaces 8 (2016) 16521–16532, https://doi.org/10.1021/acsami.6b04872.

[39] Y. Chen, X. Liu, T. Wu, W. Hou, M. Liu, Y. Zhang, S. Yao, Enhanced electrochemical sensitivity towards acetaminophen determination using electroactive self-assembled ferrocene derivative polymer nanospheres with multi-walled carbon nanotubes, Electrochim. Acta 272 (2018) 212–220, https://doi.org/10.1016/j.electacta.2018.04.019.

[40] J. Wang, Y. Gao, F. Chen, L. Zhang, H. Li, N.F. de Rooij, A. Umar, Y. Lee, P. J. French, B. Yang, Y. Wang, G. Zhou, Assembly of core/shell nanospheres of amorphous hemin/acetone-derived carbonized polymer with graphene nanosheets for room-temperature NO sensing, ACS Appl. Mater. Interfaces 14 (2022) 53193–53201, https://doi.org/10.1021/acsami.2c16769.

[41] N. Roy, K. Kannabiran, A. Mukherjee, Integrated adsorption and photocatalytic degradation based removal of ciprofloxacin and sulfamethoxazole antibiotics using Fc@rGO-ZnO nanocomposite in aqueous systems, Chemosphere 333 (2023) 138912, https://doi.org/10.1016/j.chemosphere.2023.138912.

[42] M. Bashiri, T. Zhang, Y. Gu, M.H. Sarvari, Innovative porous organic polymer incorporating ferrocene and s-triazine: an effective method for converting nitroarenes to benzimidazoles using visible light, Polymer 304 (2024) 127141, https://doi.org/10.1016/j.polymer.2024.127141.

[43] P.E. Silkoff, M. Carlson, T. Bourke, R. Katial, E. ögren, S.J. Szefler, The Aerocrine exhaled nitric oxide monitoring system NIOX is cleared by the US Food and Drug Administration for monitoring therapy in asthma, J. Allergy Clin. Immunol. 5 (2004) 1241–1256.

[44] G. Murali, M. Reddeppa, C. Seshendra Reddy, S. Park, T. Chandrakalavathi, M. Kim, I. In, Enhancing the charge carrier separation and transport via nitrogen-doped graphene quantum dot-TiO_2 nanoplate hybrid structure for an efficient NO gas sensor, ACS Appl. Mater. Interfaces 12 (2020) 13428–13436, https://doi.org/10.1021/acsami.9b19896.

[45] L.T. Duy, Y.G. Noh, H. Seo, Improving graphene gas sensors via a synergistic effect of top nanocatalysts and bottom cellulose assembled using a modified filtration technique, Sensor. Actuator. B Chem. 334 (2021) 129676, https://doi.org/10.1016/j.snb.2021.129676.

[46] S. Hou, R. Pang, S. Chang, L. Ye, J. Xu, X. Wang, Y. Zhang, Y. Shang, A. Cao, Synergistic CNFs/CoS_2/MoS_2 flexible films with unprecedented selectivity for NO gas at room temperature, ACS Appl. Mater. Interfaces 26 (2020) 29778–29786, https://doi.org/10.1021/acsami.0c05953.

[47] Y. Li, R. Pang, W. Meng, D. Zhang, M. Li, Z. Xia, J. Feng, H. Li, A. Cao, Y. Shang, Space-confined synthesis of SWNT bundles wrapped by MoS_2 crystalline layers as flexible sensors and detectors, Carbon 195 (2022) 19–26, https://doi.org/10.1016/j.carbon.2022.04.002.

[48] C. Kuchi, B. Naresh, P.S. Reddy, In situ TiO_2-rGO nanocomposite for low concentration NO gas sensor, ECS J. Solid State Sci. Technol. 10 (2021) 037008, https://doi.org/10.1149/2162-8777/abeff0.

[49] Y. Chang, F. Chen, D. Tsai, B. Kuo, F. Shieu, N-doped reduced graphene oxide for room-temperature NO gas sensors, Sci. Rep. 11 (2021) 20719, https://doi.org/10.1038/s41598-021-99883-9.

[50] J. Jeon, B. Kang, Y.T. Byun, T. Ha, High-performance gas sensors based on single-wall carbon nanotube random networks for the detection of nitric oxide down to the ppb-level, Nanoscale 11 (2019) 1587–1594, https://doi.org/10.1039/c8nr07393g.

[51] N. Lim, K.H. Kim, Y.T. Byun, Preparation of defected SWCNTs decorated with en-APTAS for application in high-performance nitric oxide gas detection, Nanoscale 13 (2021) 6538–6544, https://doi.org/10.1039/d0nr08919b.

[52] A. Hornung, D. Zemlyanov, M. Muhler, G. Ertl, The catalytic reduction of NO by H_2 on Ru(0001): observation of NH_{ads} species, Surf. Sci. 600 (2006) 370–379, https://doi.org/10.1016/j.susc.2005.10.037.

[53] J. Zeng, Y. Niu, Y. Gong, Q. Wang, H. Li, A. Umar, N.F. de Rooij, G. Zhou, Y. Wang, All-dry transferred ReS_2 nanosheets for ultrasensitive room-temperature NO_2 sensing under visible light illumination, ACS Sens. 5 (2020) 3172–3181, https://doi.org/10.1021/acssensors.0c01372.

[54] S. Nigar, H. Wang, M. Imtiaz, J. Yu, Z. Zhou, Adsorption mechanism of ferrocene molecule on pristine and functionalized graphene, Appl. Surf. Sci. 481 (2019) 1466–1473, https://doi.org/10.1016/j.apsusc.2019.03.222.

[55] E. Arunan, H.S. Gutowsky, The rotational spectrum, structure, and dynamics of a benzene dimer, J. Chem. Phys. 98 (1993) 4294–4296, https://doi.org/10.1063/1.465035.

[56] M.O. Sinnokrot, C.D. Sherrill, High-accuracy quantum mechanical studies of π-π interactions in benzene dimers, J. Phys. Chem. A 110 (2006) 10656–10668, https://doi.org/10.1021/jp0610416.

[57] A.D. Adhikari, R. Oraon, S.K. Tiwari, N.K. Jena, J.H. Lee, N.H. Kim, G.C. Nayak, Polyaniline-stabilized intertwined network-like ferrocene/graphene nanoarchitecture for supercapacitor application, Chem. Asian J. 12 (2017) 900–909, https://doi.org/10.1002/asia.201700124.

[58] T. Lu, Q. Chen, Independent gradient model based on Hirshfeld partition: a new method for visual study of interactions in chemical systems, J. Comput. Chem. 43 (2022) 539–555, https://doi.org/10.1002/jcc.26812.

[59] Y. Iizumi, H. Suzuki, M. Tange, T. Okazaki, Diameter selective electron transfer from encapsulated ferrocenes to single-walled carbon nanotubes, Nanoscale 6 (2014) 13910–13914, https://doi.org/10.1039/c4nr04398g.